Please cite the Published Version

Wei, Shengchao, Cunliffe, Alexander J, Redfern, James, Guo, Hailing and Tosheva, Lubomira (2025) Nanofiltration membranes containing CHA zeolite with pompom-like morphology. Colloids and Surfaces C: Environmental Aspects, 3. 100069 ISSN 2949-7590

DOI: https://doi.org/10.1016/j.colsuc.2025.100069

Publisher: Elsevier

Version: Published Version

Colloids and Surfaces C: Environmental Aspects 3 (2025) 100069

Contents lists available at ScienceDirect

Colloids and Surfaces C: Environmental Aspects

journal homepage: www.journals.elsevier.com/colloids-and-surfaces-c-environmental-aspects

Nanofiltration membranes containing CHA zeolite with pompom-like morphology

Shengchao Wei [a], Alexander J. Cunliffe [b], James Redfern [b], Hailing Guo [a,*], Lubomira Tosheva [b,*]

[a] State Key Laboratory of Heavy Oil Processing, College of Chemical Engineering, China University of Petroleum (East China), Qingdao, Shandong 266580, PR China
[b] Faculty of Science and Engineering, Manchester Metropolitan University, Chester Street, Manchester M1 5GD, United Kingdom

ARTICLE INFO

Keywords:
CHA zeolite
Zeolite morphology
TFC NF membranes
Antibacterial

ABSTRACT

Thin-film composite (TFC) nanofiltration membranes are widely used for water treatment due to their energy efficiency and high salt rejection, however they are highly susceptible to biological fouling. CHA zeolite with pompom-like morphology was prepared from an organic structure-directing template-free synthesis gel in the presence of sodium and cesium. The zeolite was added to the polyamide (PA) layer of TFC membranes prepared via interfacial polymerization. M-0.01 and M-0.05 TFC membranes prepared with addition of 0.01 wt% and 0.05 wt% CHA zeolite to the aqueous piperazine monomer solution, displayed a thinner PA layer and higher permeability compared to zeolite-free M-0 membranes. The rejection of 2000 ppm Na_2SO_4 and $MgSO_4$ solutions of the M-0.05 membrane was slightly reduced compared to M-0 and M-0.01 but nevertheless remained higher than 90%. Ag-CHA zeolite suspensions showed antibacterial activity against *Escherichia coli*, whereas CHA zeolite was inactive. Following bacterial exposure, M-0 control membranes exhibited bacterial growth after 24 h compared to the 0 h count, which was not observed for M-0.05 membranes, where there was no significant difference in the count between 0 h and 24 h. As a bacterial population reduction was not observed in either case, these materials are considered not to be antimicrobial. No bacteria survived on the surface of Ag-treated M-0 and M-0.05 membranes, demonstrating antimicrobial activity. The methodology described in this work could be used to increase the resistance of TFC membranes to biological fouling and increase their operational lifetime.

1. Introduction

Zeolites are microporous aluminosilicate materials with regular pores and channels and high surface areas, which are conventionally used in many commercial catalytic, separation, and ion-exchange processes [1]. In addition, they have shown potential for emerging technologies to address environmental challenges such as air and water quality and climate change [2–4]. Conventionally, zeolites are synthesized by hydrothermal treatment of aluminosilicate gels or solutions in an alkaline medium [5]. The quest to expand existing zeolite structures and zeolite structural compositions has led to the use of organic structure-directing agents (OSDAs) in zeolite syntheses. Despite the successes in preparing new structures and extended zeolite compositions, OSDA-mediated zeolite syntheses are often not suitable for mass production due to cost, energy consumption, gas emissions and waste generation, which are mostly related to the synthesis of OSDAs themselves and post-synthesis OSDA removal by calcination [6]. Increasing understanding of the zeolite crystallization mechanism and efforts to make zeolite syntheses more sustainable have resulted in revitalized research interest in the use of cations such as Na^+, K^+ and Cs^+ as inorganic structure-directing agents for zeolite crystallization [7–14]. We have recently reported the synthesis of a novel Cs-Na EDI-type zeolite, zeolite MMU-1, in the presence of Na^+ and Cs^+ inorganic structure-directing cations [15]. MMU-1 was composed of aggregated nanocrystals with sizes in the range 20–40 nm. Here, we have systematically varied the sodium and cesium content in the MMU-1 zeolite precursor gel with the aim of preparing zeolites with morphologies that are suitable for nanofiltration membrane applications.

Membrane separation processes have been widely used for water purification and desalination [16,17]. Among different membrane families, the thin-film composite (TFC) nanofiltration (NF) membranes have been broadly applied in water treatment due to their energy efficiency and excellent ion selectivity [18]. TFC NF membranes are prepared via interfacial polymerization (IP) of active monomers such as

---

* Corresponding authors.
E-mail addresses: guohl@upc.edu.cn (H. Guo), l.tosheva@mmu.ac.uk (L. Tosheva).

https://doi.org/10.1016/j.colsuc.2025.100069
Received 4 February 2025; Received in revised form 9 April 2025; Accepted 9 April 2025

piperazine (PIP) and trimesoyl chloride (TMC), which results in the formation of a thin polyamide (PA) layer on a porous substrate [19,20]. The structural properties of the PA layer determine the separation performance of the TFC membrane. However, the high reactivity of PIP and TMC monomers often leads to the formation of a thicker PA layer with increased mass transfer resistance [21,22]. Breaking the trade-off between water permeability and ion selectivity has been demonstrated to be challenging [23]. Thus, designing a TFC membrane with enhanced permeability and high selectivity is highly desirable for water treatment applications.

Over the past two decades, numerous strategies have been used to tailor the membrane structure for improving membrane separation performance, such as design of monomers with tailored functionalities, incorporating additives into the PA layer or constructing a nanoporous interlayer between the PA and the porous substrate [24–30]. Among different inorganic nanofillers, the introduction of nanozeolites in the PA layer has been recognized as an effective strategy to regulate the membrane structure and improve membrane performance [31–33]. The superior performance of such thin-film nanocomposite (TFN) membranes containing zeolite nanofillers has been attributed to zeolites' tunable hydrophilicity, large surface areas and regular pore structures, negative framework, and high chemical, thermal and mechanical stability. The use of zeolites that have been ion-exchanged with Ag introduced antifouling capability of the TFC membranes prepared [34], which addresses one of the main drawbacks of nanofiltration membranes, namely their susceptibility to biological degradation and the need for periodic chemical cleaning. The latter causes interruption in operation, increase in cost and, most importantly, damages the PA layer in the long term [16,35].

The aims of the present work were to incorporate CHA zeolite with pompom-like morphology, which was synthesized in an OSDA-free system in the presence of Na and Cs, in TFC NF membranes, and evaluate the permeability and selectivity of the obtained TFN membranes. Additionally, this paper describes the post-fabrication loading of Ag within the membrane [36] and presents results for the antibacterial efficacy of Ag-treated TFC membranes.

2. Materials and methods

2.1. Zeolite synthesis and characterization

Zeolites MMU-1, RHO and CHA were prepared from gels with the molar composition $10SiO_2$: $2.2Al_2O_3$: xNa_2O: yCs_2O: zH_2O, where $x = 23$ (MMU-1), 13 (RHO) or 8.1 (CHA), $y = 1.4$ (MMU-1) or 0.7 (RHO and CHA), and $z = 382$ (RHO and CHA) or 383 (MMU-1), following the procedure described in ref. [15]. The precursor gels were prepared by dissolving 1.03 g sodium aluminate ($NaAlO_2$, 50.5% Al_2O_3, 44.1% Na_2O, Fisher Scientific) in 12.42 g distilled water in a beaker under stirring. The beaker was placed in a large Petri dish with cold water to keep the temperature constant upon the addition of sodium hydroxide (NaOH pellets, analytical reagent grade, Fisher Scientific) (3.64 g, 1.82 g, or 0.91 g) and cesium hydroxide hydrate ($CsOH{\cdot}xH_2O$, 99.9%, 15 −20% H_2O, Alfa Aesar) (1.18 g or 0.59 g). After complete dissolution of the hydroxides, 4.46 g of colloidal silica (Ludox HS-30, Aldrich) were added dropwise, and the mixture was stirred for 2 h. After the stirring, the gels were transferred to 125 mL polypropylene reactors and hydrothermally treated at 80 °C for 20 h (MMU-1) or 22 h (RHO and CHA). The zeolites obtained were purified by three-times centrifugation and redispersion in distilled water and dried at 80 °C overnight. Finally, the samples were grinded and stored in glass vials at ambient conditions.

The CHA zeolite selected for the preparation of TFC membranes was upscaled using analogous procedure but with four times the amount of each chemical and a 500 mL polypropylene reactor was used for the hydrothermal treatment. This sample was labelled as CHA-4× . The zeolite yield of CHA-4× was calculated from the ratio of the mass of SiO_2 in the zeolite product and in the gel [37]. A portion of this sample (1.2 g) was ion-exchanged with 120 g of 0.01 M silver nitrate ($AgNO_3$, 99+%, Alfa Aesar) aqueous solution. The ion-exchange was performed in a 150 mL beaker covered with Al foil; the sample was stirred in the Ag solution for 24 h at room temperature, followed by three-times centrifugation and redispersion in distilled water and drying at 80 °C overnight. The obtained Ag-CHA-4× was stored in a glass vial covered with foil.

Crystalline phases were determined from X-ray diffraction (XRD) patterns collected with a PANalytical X'pert Powder X-ray diffractometer using Cu Kα$_1$ radiation ($\lambda = 0.$ 1.5406 Å) and a PIXCel 1-D detector. Data were collected in the range 5–50° 2θ with a step size of 0.013° 2θ and a measuring time of 89 s per step. The samples were rotated at 60 rpm during the data collection. Crystallite sizes of CHA and CHA-4× were determined using the Size/Strain calculator incorporated into PANalytical Data Viewer with the instrumental broadening function determined using a NIST SRM674b CeO_2 external standard. The morphology of the zeolites prepared was studied with a scanning electron microscope (SEM) (Carl Zeiss Supra 40 V). Samples were sputtered with gold prior to analysis. The chemical composition of the samples was determined using an X-ray fluorescence (XRF) instrument (Rigaku NEX-CG energy-dispersive X-ray fluorescence spectrometer). Nitrogen adsorption isotherm measurements at −196 °C were performed with a Micrometrics ASAP 2020 surface area analyzer. Samples were degassed at 300 °C overnight prior to analysis. The Brunauer–Emmett–Teller (BET) method was used to calculate the samples' surface areas and Barrett–Joyner–Halenda (BJH) pore-size distributions were determined from the desorption branch of the isotherms. Micropore volumes and external surface areas were determined by the t-plot method, whereas total pore volumes were calculated from the volume adsorbed at a relative pressure of 0.99.

2.2. Fabrication and characterization of TFC and TFN membranes

The TFC and TFC-zeolite NF membranes were constructed on polyethersulfone (PES) porous substrates (Haiyan Xindongfang Suhua Co., Ltd., effective pore size of 100 nm) through IP reaction. Firstly, 0 wt%, 0.01 wt% or 0.05 wt% of CHA-4× were added to 0.1 wt% PIP (TCI (Shanghai)) aqueous solution. The PES membranes were fixed in a plastic frame and immersed in the PIP or PIP-zeolite solutions for 60 s. The residual PIP solution on the membrane surface was removed by a roller. Subsequently, 0.15 wt% of TMC (TCI (Shanghai)) n-hexane solution (≥ 97%, AR) was poured onto the PES membrane surfaces to start the IP process. After a reaction for 60 s, the residual solution was removed. The obtained membranes were transferred to an oven at 60 ℃ and dried for 20 min. The membranes were placed into deionized (DI) water prior to use. The zeolite-free TFC membrane was named as M-0, whereas the zeolite-containing TFN membranes were labelled as M-0.01 and M-0.05, respectively, according to their zeolite content in the PIP aqueous solution.

The desalination performance of the TFC NF membranes was evaluated on a crossflow equipment. Inorganic salts (Na_2SO_4 and $MgSO_4$, 2000 $\mu g\ g^{-1}$) were used as the feed solutions. After pre-pressurizing at 3 bar for 1 h, the permeate was collected and recorded. The concentration of salts solutions was determined by a conductivity meter. The permeance (J, $L\ m^{-2}\ h^{-1}\ bar^{-1}$) and the salt rejection (R, %) were measured and calculated by Eq. (1) and Eq. (2), respectively.

$$J = \frac{Q}{P \quad \Delta t \quad A} \tag{1}$$

$$R = \left(1 - \frac{C_P}{C_f}\right) \times 100\% \tag{2}$$

where Q, A, P, and Δt are the permeate volume (L), membrane testing area (m^2), operating pressure (bar), and testing time (h), respectively; C_p and C_f are the salt concentration of permeate and feed.

The molecular weight cut-off (MWCO and pore properties of prepared membranes were measured by solute transport method using different molecular weight of test PEG (polyethylene glycol, AR, Sinopharm) solutions (200, 300, 400, and 600 Da) [38]. The morphology and the thickness of the membranes were measured by SEM (JEOL-7900F, Japan). The morphology and the thickness of the membranes were measured by SEM (JEOL-7900F, Japan).

Further, TFC and TFC-CHA zeolite membranes were treated with 0.01 M silver nitrate solutions according to our previous protocol with modifications [36]. Individual M-0 and M-0.05 membranes (5 cm in diameter) were placed in 250 mL beakers, and 20 mL 0.01 M $AgNO_3$ solutions were added to each beaker. The beakers were covered with parafilm and Al foil and left at room temperature for 24 h. Next, each membrane was washed with distilled water (20 times), kept in distilled water for 48 h, washed again and dried at 50 °C overnight.

2.3. *Antimicrobial efficacy assessment*

2.3.1. *Bacterial suspensions*

Saline (0.85% sodium chloride, OXOID), tryptone soya agar (TSA, OXOID) plates, DE broth (Remel) and nutrient broth (OXOID) were prepared according to the manufacturer's instructions. Soya casein digest lecithin polysorbate (SCDLP) neutralizer was created by adding 30 g L^{-1} tryptone soya broth (TSB, OXOID), 1 g L^{-1} L-α-lecithin (Acros organics) and 7 g L^{-1} polysorbate 80 (Acros organics) to distilled water and sterilizing by autoclave at 121 °C for 15 min. A suspension of *Escherichia coli* (*E. coli*) ATCC 8545 was created by streaking one loop from a −80 °C stock to a TSA plate and incubating at 37 °C for 24 h, then re-streaking one colony to a new TSA plate and incubating in the same manner. Several colonies were then transferred to 10 mL saline.

2.3.2. *Antimicrobial efficacy of zeolite suspensions*

The *E. coli* suspension was adjusted to 0.1 ± 0.005 OD at 600 nm using a spectrophotometer (Jenway 6305, UK), to form a final concentration of $\sim 1 \times 10^8$ cells mL^{-1}. Suspensions of CHA-4× and Ag-CHA-4× zeolites with concentrations of 1 and 2 mg L^{-1} were prepared in 9 mL sterile saline and vortexed for a minimum of 60 s. For neutralization and to assess bacterial survival, 900 μL of DE broth were aliquoted into six triplicate groups for each compound (18 aliquots of DE broth per compound suspension). One hundred microliters of bacterial culture were transferred by pipette into each compound suspension and a timer started at the time of inoculation. Immediately after inoculation, each culture was vortexed for 5 s and then 100 μL transferred in triplicate to DE broth. After 5, 10-, 20-, 30-, and 40-min post-inoculation, the process was repeated. All DE broth suspensions were then incubated at 37 °C for 24 h and observed for color change (purple to gold), where a color change demonstrates bacterial survival and growth. In addition, quantification via spread plate (100 μL) was performed for each neutralized solution immediately after inoculation and homogenization, followed by incubation at 37 °C for 24 h.

2.3.3. *Antimicrobial efficacy of Ag-treated TFC NF membranes*

A modified version of ISO 22,196 was used to test the antimicrobial efficacy of the Ag-treated TFC membranes that come into contact with bacteria. To achieve this, an *E. coli* suspension was adjusted to 0.5 ± 0.01 OD at 600 nm, then serially diluted 1: 9 twice to form a final concentration of $\sim 1\text{–}5 \times 10^6$ cells mL^{-1}. M-0 and M-0.05 membranes, as well as Ag-treated M-0 and M-0.05 membranes were cut into sections of 2 cm x 2 cm and sterilized by ultraviolet light in a UV crosslinker for 30 min. Six coupons of each material were inoculated with 100 μL of suspension and either immediately recovered into 5 mL SCDLP neutralizer or incubated at 35 °C for 24 h at > 90% relative humidity. After recovery, the membranes were manually agitated to dislodge cells into the neutralizer, then the neutralizer was transferred to a 30 mL universal tube, vortexed to homogenize, serially diluted 1: 9 to 10^{-2} and quantified via spread plate on TSA in triplicate.

3. Results and discussion

3.1. *Zeolite synthesis*

In our previous work, variations of the molar composition of the zeolite precursor gel led to the synthesis of a new Cs-Na modification of EDI-type zeolite [15]. The presence of Cs as well as the water content were found to have a crucial role for the type of zeolite formed. We have now varied systematically the amount of sodium hydroxide and cesium hydroxide hydrate added to the zeolite precursor gel and kept the SiO_2/Al_2O_3 ratio and the synthesis conditions the same. Zeolites MMU-1, RHO and CHA crystallized from the different molar compositions used (Fig. 1a). All zeolites were composed of aggregated nanoparticles, however, there were distinct differences between the morphologies of the three zeolites (Fig. 1b). MMU-1 was composed of 20–70 nm primary nanoparticles, which were further arranged into loose irregular clusters with sizes of up to 500 nm. Zeolite RHO contained well-faceted intergrown rectangular primary nanocrystals, which built up the large, up to 1.5 μm in diameter dense spherical particles observed in the SEM images. Smaller (400–700 nm) and less dense spherical particles made up of spherical nanoparticles were present in this sample too. The latter could be due to the presence of CHA impurities, as seen by the presence of an extra broad peak at around 30 degrees two theta in the XRD pattern of RHO (Fig. 1a). Finally, zeolite CHA displayed pompom-like particles with sizes in the range 900 nm - 1.5 μm built up of distinct nanocrystals.

The amount of NaOH and $CsOH{\cdot}xH_2O$ used to prepare the different zeolite precursor gels as well as XRF data are depicted in Table 1. The results for two additional syntheses, which produced RHO and CHA samples of lower crystallinity / purity (samples labelled as RHO* and CHA*), are also included in the table, whereas XRD patterns of these two samples are shown in Fig. S1, Supplementary material. The amount of sodium hydroxide and cesium hydroxide hydrate added to the precursor gel was the only difference between the different samples prepared. The role of alkali cations for zeolite crystallization is dual – they can act as both mineralizing agents and as inorganic structure-directing agents, and it is often challenging to distinguish between the two effects [8]. We have demonstrated previously that the synthesis using the MMU-1 precursor gel without addition of Cs resulted in SOD [15]. This result suggested a cooperative Cs-Na structure direction mechanism [8]. The results reported here further support this finding. Considering the relative ratio of Na and Cs hydroxides added to the precursor gels, it seems that the amount of NaOH hydroxide in combination with a certain amount of Cs determined the type of zeolite formed (Table 1). Variations in the Cs content further influenced the purity of the zeolite products formed. Interestingly, more Cs than Na was present in all product samples, despite its lower content in the precursor gel for all but the CHA* sample. The alkalinity of the precursor gels decreased in the order MMU-1 >RHO* >RHO>CHA* >CHA. The Si/Al ratio increased from MMU-1 to RHO and CHA as expected [11]. Furthermore, the Si/Al ratio of all samples was below 2, in agreement with previous results for template-free zeolites using similar precursor gels [12,13,15]. RHO*- and CHA*samples did not match the trends, but this could be because the samples are not well-crystallized / contained other phases, as seen from their SEM images (Fig. S1, Supplementary information). The result for zeolite CHA is particularly interesting. Firstly, the synthesis of CHA in the absence of K has rarely been reported [8]. For instance, Mintova and co-workers have shown that zeolite CHA could not be formed in the absence of K and could only be prepared using a mixture of three cations, Na, K and Cs [13]. Here, we show that CHA can be prepared in the absence of K by adjusting the Na and Cs concentration in the precursor gel. Another benefit of the zeolite CHA prepared is its distinct pompom-like morphology. Sunflower-like CHA zeolite prepared in the presence of an organic template, has shown superior CO_2 adsorption capacity and CO_2/N_2 and CO_2/CH_4 selectivity compared to conventional zeolites [39].

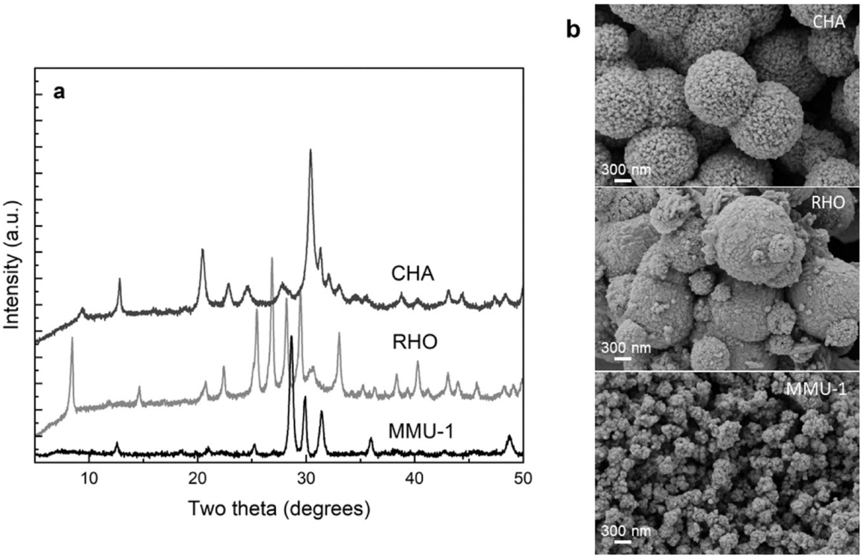

Fig. 1. (a) XRD patterns and (b) SEM images of the zeolites prepared using precursor gels with different molar compositions: MMU-1 ($10SiO_2$: $2.2Al_2O_3$: $23Na_2O$: $1.4Cs_2O$: $383H_2O$), RHO ($10SiO_2$: $2.2Al_2O_3$: $13Na_2O$: $0.7Cs_2O$: $282H_2O$) and CHA ($10SiO_2$: $2.2Al_2O_3$: $8.1Na_2O$: $0.7Cs_2O$: $282H_2O$).

Table 1
Zeolite types prepared, amount of NaOH (g) and $CsOH{\cdot}xH_2O$ (g) added to the precursor gels, and XRF data for Si/Al, Cs/Na, Cs/Si, Cs/Al, Na/Si and Na/Al ratios in the zeolite products.

Zeolite	NaOH	$CsOH{\cdot}xH_2O$	Si/Al	Cs/Na	Cs/Si	Cs/Al	Na/Si	Na/Al
MMU−1	3.64	1.18	1.09	1.43	1.08	1.17	0.81	0.75
RHO	1.82	0.59	1.44	1.02	0.56	0.81	0.79	0.55
RHO*	1.82	1.18	1.45	1.93	0.95	1.38	0.49	0.71
CHA	0.91	0.59	1.78	1.32	0.55	0.98	0.74	0.42
CHA*	0.91	1.18	1.83	3.91	1.18	2.16	0.30	0.55

We have selected the pompom-like CHA zeolite for incorporation into TCF NF membranes due to its spherical morphology and nanocrystal arrangement. The CHA synthesis was upscaled and comparison between zeolite products of the 1x (starting with 1.03 g $NaAlO_2$) and 4x (starting with 4.12 g $NaAlO_2$) syntheses is shown in Fig. 2. The zeolite phase, sample morphology, Si/Al ratio and textural characteristics (Table 2) are generally preserved in the upscaled product (CHA-4×), although some minor differences were observed. The latter could be due to the different size of polypropylene reactors used in the two syntheses, 125 mL versus 500 mL, and differences in the pressure inside [40]. The surface area of both CHA zeolites was below 100 m^2g^{-1} indicating that the presence of Cs cations restricted the access of nitrogen, which agreed with the results reported by Debost et al. [13]. The isotherms contained a hysteresis loop, which was also like the isotherm reported in ref. [13]. The higher total pore volume of the Na,Cs-CHA samples in this work and the variations in the other textural characteristics compared to the CHA zeolite prepared in the presence of Na, K and Cs cations [13] are due to differences in the type and the number of extra-framework cations. The weight of CHA-4× purified sample was 9.22 g, and XRF data indicated that its SiO_2 content was 50.5 wt%. Therefore, the yield was calculated as: $yield = \frac{9.22\times0.505}{18.64\times0.3}\times 100 = 83.3\%$.

3.2. TFN NF membranes

TFN NF membranes were prepared with the addition of CHA-4× at two different weight ratios to the PA layer. Top view SEM images of PES, M-0, M-0.01 and M-0.05 membranes are shown in Fig. 3. The M-0 membrane displayed a classical nodular-structure morphology compared to the porous morphology of PES [29]. After introducing zeolite, the zeolite crystals could be seen evenly distributed on the surface of M-0.01 membrane (Fig. 3c). Further increase in the zeolite loading resulted in aggregated and interconnected zeolite clusters on the surface of M-0.05 (Fig. 3d). The pompom-like morphology of the CHA zeolite with its rich surface texture seems to form a tighter interface with the polyamide layer in M-0.05, which is beneficial for enhancing the water permeance.

Fig. 4 depicts the effect of the zeolite loading on the thickness of the PA layer in TFC membranes. The thickness of the PA layer in the control M-0 membrane was 76 ± 9 nm (Fig. 4a). After doping with zeolite, the thickness of the PA layer decreased to 50 ± 4 nm (M-0.01 membrane, Fig. 4b) and 44 ± 5 nm (M-0.05 membrane, Fig. 4). The presence of a porous zeolite can restrict the diffusion of the PIP monomer towards the interface due to adsorptive interactions. The restricted diffusion of PIP to the organic interface leads to an inadequate supply of PIP during subsequent reactions with TMC, thereby impeding the vertical growth of the PA network and ultimately resulting in a reduced thickness of the mature PA membrane [28,41]. The reduction of the membrane's thickness is beneficial for decreasing the transport resistance of water and enhancing the water permeability [30]. Furthermore, the incorporation of CHA zeolites in TFN membranes can provide a fast, low-energy path for water, further improving the water flux of the membrane.

As shown in Fig. 5, the MWCO of M-0 and M-0.05 membrane were 446 and 529 Da, respectively. This result indicates that the zeolite incorporation increases the pore size of the M-0.05 membrane compared to the control M-0 membrane. The introduction of porous zeolite in the aqueous PIP solution inhibits the diffusion of PIP, thereby limiting the full reaction of IP, damaging the cross-linked structure of the PA layer and increasing the pore size of the membrane.

The water permeance of the M-0 membrane was 7.2 $L{\cdot}m^{-2}{\cdot}h^{-1}{\cdot}bar^{-1}$, and its rejection of Na_2SO_4 was 95.4% (Fig. 6a). After introducing zeolite, the water permeance of M-0.01 and M-0.05 membrane increased to 10.1 $L{\cdot}m^{-2}{\cdot}h^{-1}{\cdot}bar^{-1}$ and

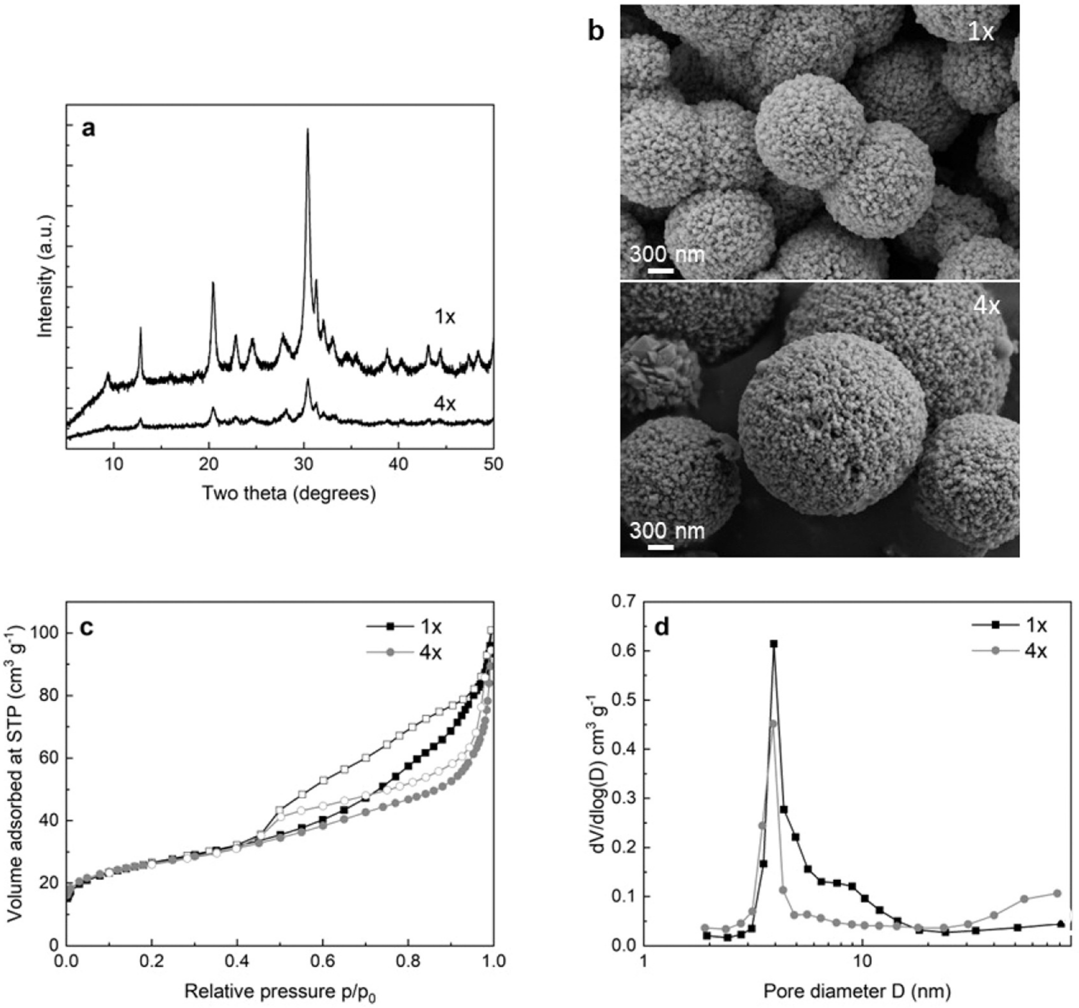

Fig. 2. Comparison between zeolite CHA synthesized using 1 × and 4 × quantities of the starting raw materials: (a) XRD patterns, (b) SEM images, (c) nitrogen adsorption-desorption isotherms (solid symbols, adsorption; open symbols, desorption), and (d) corresponding pore-size distributions.

Table 2
Si/Al ratios, BET (S_{BET}) and external (S_{EXT}) surface areas, micropore (V_{μ}) and total (V_{TOTAL}) pore volumes and crystallite sizes of CHA zeolites synthesized using 1 × and 4 × quantities of the starting raw materials.

Zeolite	Si/Al	S_{BET}, m^2 g^{-1}	V_{μ}, cm^3 g^{-1}	S_{EXT}, m^2 g^{-1}	V_{TOTAL}, cm^3 g^{-1}	Crystallite size, Å
CHA−1 ×	1.78	92.0	0.011	68.8	0.16	200
CHA−4 ×	1.77	90.4	0.015	58.8	0.15	170

14.3 $L \cdot m^{-2} \cdot h^{-1} \cdot bar^{-1}$, correspondingly. This increase is consistent with results reported in the literature for zeolite-containing NF membranes [31]. The enhanced permeability of the composite CHA membrane can be attributed to two factors. On the one hand, the porous zeolite optimizes the transport path within the composite membrane and accelerates the rapid transfer of water molecules. On the other hand, the porous zeolite influences the IP process, which results in reduced thickness of the composite membrane, and therefore reduced mass transfer path.

Meanwhile, compared to M-0 membrane, the rejection of Na_2SO_4 of M-0.01 membrane was 95.6%, but that of M-0.05 membrane was 92.0% (Fig. 6a). This indicates that the excessive zeolite loading in the PA membrane reduces the selectivity of NF membranes due to zeolite aggregation leading to membrane defects. The water permeance and selectivity of M-0, M-0.01 and M-0.05 for Mg_2SO_4 showed the same trends (Fig. 6b). The presence of CHA zeolite on the surface of the PA layer led to the enhanced water permeability of the membranes because of the additional channels for water to flow provided by the hydrophilic porous zeolite.

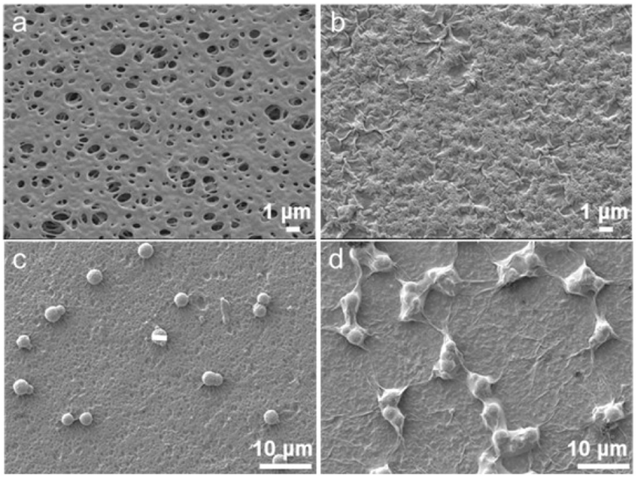

Fig. 3. Top-view SEM images of (a) PES, (b) M-0, (c) M-0.01, and (d) M-0.05 membrane.

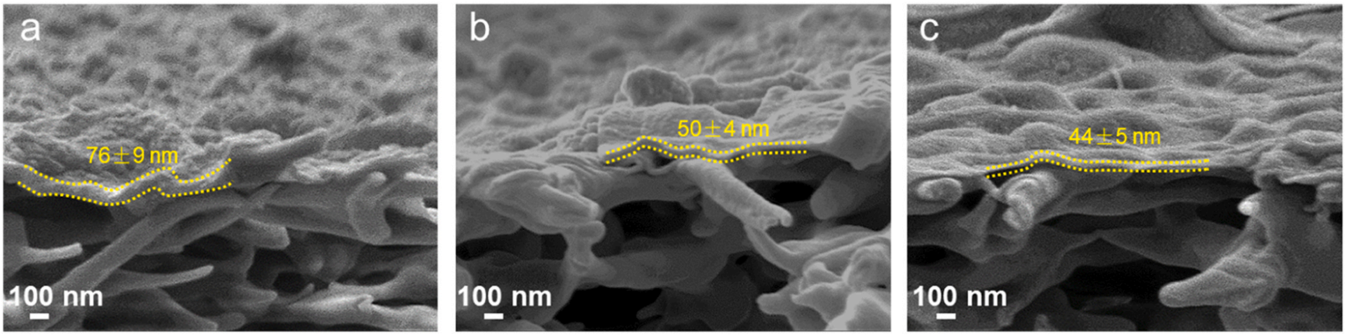

Fig. 4. Cross-section SEM images of (a) M-0, (b) M-0.01, and (c) M-0.05 membranes.

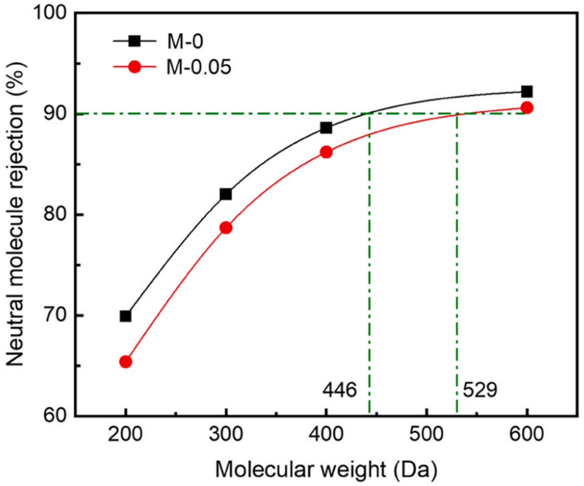

Fig. 5. PEG rejection curves and MWCO of M-0 and M-0.05 membranes.

3.3. Antibacterial efficacy of CHA zeolite suspensions and TNF membranes

It is well-known that as-made zeolites do not have any antimicrobial properties but introducing metals such as Ag and Cu into zeolites by ion-exchange create antimicrobial activity against a wide-range of micro-organisms [42,43]. For Ag zeolites, we have demonstrated that the antibacterial efficacy depends on the zeolite concentration and zeolite type, and it is not proportional to the silver concentration within the zeolite [42]. The antibacterial efficacy of CHA-4× and Ag-CHA-4× zeolite suspensions of two different concentrations was studied and results are presented in Table 3. DE neutralizing broth is a broad-spectrum chemical neutralizer used to stop antimicrobial activity at defined time points. Whilst previously we have used neutralizing agar, where antimicrobial activity was stopped at the point of spreading bacteria onto the agar [42,43], using neutralizing broth is a quicker process, making the data more realistic of the time point at which the sample was taken [44]. Sample Ag- CHA-4× contained 7.75 wt% Ag according the XRF analysis. No bacterial growth was observed in any uninoculated suspension (controls). Bacterial growth (color change of DE neutralizer broth) was observed in both inoculated concentrations of zeolite CHA at all time points. However, bacterial growth in the presence of 1 mg mL^{-1} Ag-CHA zeolite was only demonstrated up to 20 min incubation and growth was only demonstrated in the presence of 2 mg mL^{-1} zeolite up to 10 min incubation. Presence or absence of growth based on color change of DE neutralizer broth were confirmed by

Table 3

Growth (Ve+) or absence of growing bacteria (Ve-) over time in the presence of CHA or Ag-CHA zeolites (concentrations of 1 mg mL^{-1} or 2 mg mL^{-1}) and test conditions (with or without *E. coli*).

	Time (min)					
Sample	0	5	10	20	30	40
CHA 1 mg mL^{-1}	Ve-	Ve-	Ve-	Ve-	Ve-	Ve-
CHA 1 mg mL^{-1} *E. coli*	Ve+	Ve+	Ve+	Ve+	Ve+	Ve+
CHA 2 mg mL^{-1}	Ve-	Ve-	Ve-	Ve-	Ve-	Ve-
CHA 2 mg mL^{-1} *E. coli*	Ve+	Ve+	Ve+	Ve+	Ve+	Ve+
Ag-CHA 1 mg mL^{-1}	Ve-	Ve-	Ve-	Ve-	Ve-	Ve-
Ag-CHA 1 mg mL^{-1} *E. coli*	Ve+	Ve+	Ve+	Ve-	Ve-	Ve-
Ag-CHA 2 mg mL^{-1}	Ve-	Ve-	Ve-	Ve-	Ve-	Ve-
Ag-CHA 2 mg mL^{-1} *E. coli*	Ve+	Ve+	Ve-	Ve-	Ve-	Ve-

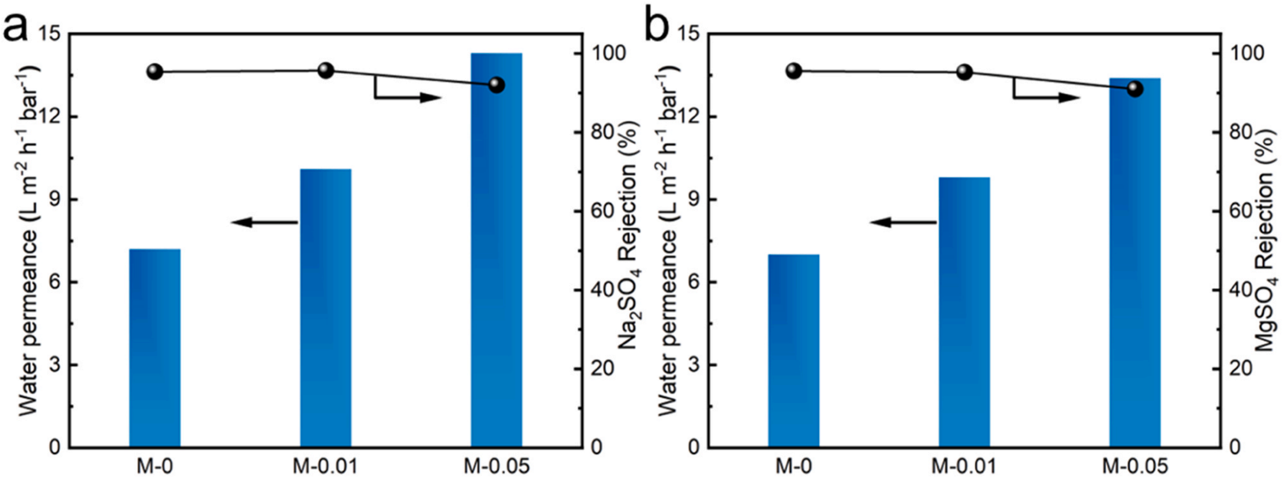

Fig. 6. Separation performance of M-0, M-0.01 and M-0.05 membranes for (a) Na_2SO_4 and (b) $MgSO_4$ salt solutions (2000 ppm).

spread plates, where all samples demonstrating absence of growing bacteria were confirmed to be a complete reduction of viable bacterial populations.

Following the establishment of bactericidal activity of Ag-CHA, tests were performed with TFC, CHA-TFC, and corresponding Ag-treated TFC membranes (M-0 and M-0.05, Fig. 7). For M-0 and M-0.05 membranes, an initial concentration of 5.44×10^4 CFU / coupon was recovered from the control M-0 coupons and 5.61×10^4 CFU / coupon on the zeolite M-0.05 coupons, with no statistically significant difference observed ($p > 0.9999$). After 24 h, statistically significant ($p = 0.0019$) growth was observed on the control coupons to 1.21×10^6 CFU / coupon, while no statistically significant difference ($p = 0.9998$) was observed after 24 h on the zeolite coupons (7.30×10^4 CFU / coupon). While a difference in the control and zeolite coupons was observed after 24 h, a bacterial reduction did not occur on either surface, indicating the lack of antimicrobial action on these control surfaces. For Ag-treated membranes, an initial concentration of 7.61×10^4 CFU / coupon was recovered from the control Ag-M-0 coupons and 5.22×10^4 CFU / coupon on the zeolite Ag-M-0.05 coupons, with a statistically significant difference observed ($p = 0.0379$). After 24 h, both Ag-M-0 and Ag-M-0.05 recovered zero CFU.

The observed bacterial growth on the control membranes, which was not observed for the zeolite-containing membranes indicates that the zeolite could offer a degree of protection against biological fouling. However, further experiments under real-life conditions are needed to confirm these results and to establish the potential protection mechanism. The results with Ag-treated membranes showed that this is an efficient method to eliminate bacteria. In our previous work on dental acrylic (DA) resins and zeolite-containing DA resins, we have demonstrated that the addition of Ag-exchanged zeolites prior to polymerization resulted in Ag^+ reduction to elemental silver and resin colorization [36]. This was circumvented by performing the Ag ion-exchange within the zeolite after the fabrication of the Na-zeolite-DA resins. However, it was established that the as described Ag treatment also resulted in non-zeolitic silver adsorbed onto the resin, which could be removed after 2-days incubation of the DA coupons in distilled water. We have used a similar procedure to treat the M-0 and M-0.05 membranes with silver in this work. The results in Fig. 7b indicate that the 2-days incubation of the membranes in distilled water was not enough to remove the non-zeolitic silver from the membranes. This could be due to the presence of a negatively charged outer layer in the PA film, attracting the positively charged Ag ions [42]. Nevertheless, the results reported suggest that post-fabrication of zeolite-containing TFC NF membranes could be an efficient way to reduce the frequency of membrane's chlorine treatment to eliminate biological fouling and thus to extend the lifetime of NF membranes.

4. Conclusion

MMU-1, RHO and CHA zeolites were prepared from OSDA-free zeolite precursor gels in the presence of NaOH and $CsOH \cdot xH_2O$. A cooperative Na-Cs structure-direction to corresponding zeolite structures was observed. Among the different zeolites prepared, CHA zeolite composed of well-faceted nanocrystals arranged into pompom-like spherical particles was selected for incorporation into thin-film composite nanofiltration membranes. The performance of M-0.01 and M-0.05 membranes containing 0.01 wt% and 0.05 wt% CHA zeolite added to the aqueous PIP monomer solution was compared to control M-0 membranes, which did not contain a zeolite. The membrane's permeability increased with an increase in the zeolite content, however, the Na_2SO_4 and $MgSO_4$ rejection of M-0.05 was slightly reduced compared to M-0 and M-0.01 due to zeolite aggregation leading to membrane defects. The membranes were tested for their antibacterial efficacy against *E. coli*. Bacterial growth was observed after 24 h for M-0, which was not the case for M-0.05. No bacteria survived on the surface of both type of membranes after treatment with 0.01 M $AgNO_3$ solution. The results indicate that the methodology described could be potentially applied to reduce biological fouling of TFC membranes after long-term assessment of the membranes antibacterial resistance.

CRediT authorship contribution statement

Tosheva Lubomira: Writing – review & editing, Writing – original draft, Visualization, Validation, Methodology, Funding acquisition, Conceptualization. **Guo Hailing:** Writing – review & editing, Supervision, Funding acquisition. **Redfern James:** Writing – review & editing, Supervision. **Cunliffe Alexander J:** Writing – review & editing, Visualization, Methodology, Investigation, Formal analysis. **Wei Shengchao:** Writing – review & editing, Visualization, Methodology, Investigation, Formal analysis.

Funding sources

This work was supported by The Royal Society, UK [grant number IEC\NSFC\211137], National Key Research and Development Program of China (No. 2024YFE0206800), and High-End Foreign Experts Introduction Project (G2023152003L). LT is grateful to Mohammad Akmal Mahmood for their contribution to the zeolite syntheses. JR thanks

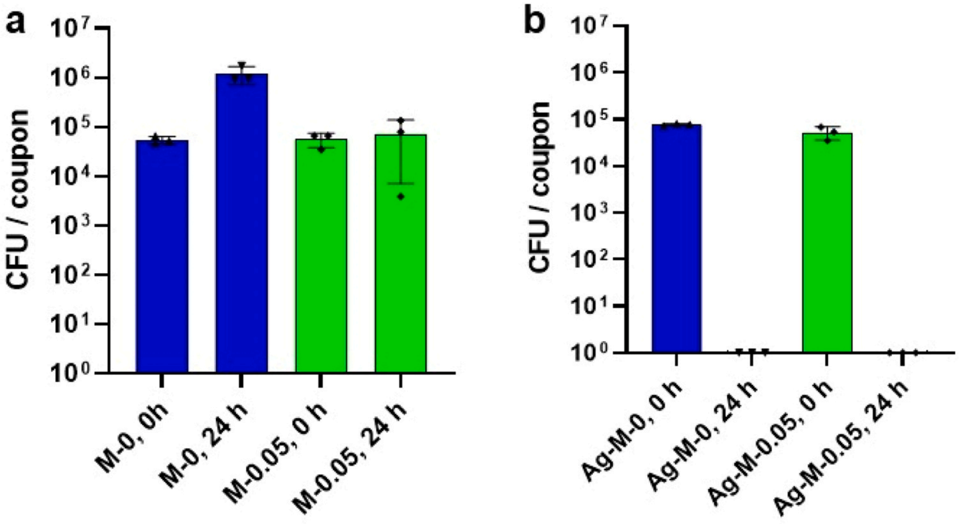

Fig. 7. Antibacterial efficacy of (a) M-0 and M-0.05 membranes and (b) Ag-treated M-0 and M-0.05 membranes.

Michaella Morris who helped develop the testing methodology for the antimicrobial efficacy assessment.

Declaration of Competing Interest

The authors declare that they have no known competing financial interests or personal relationships that could have appeared to influence the work reported in this paper.

Appendix A. Supporting information

Supplementary data associated with this article can be found in the online version at doi:10.1016/j.colsuc.2025.100069.

Data availability

Data will be made available on request.

References

[1] D.W. Breck, Zeolite Molecular Sieves: Structure, Chemistry, and Use, John Wiley & Sons Inc, New York, 1974.

[2] D.G. Boer, J. Langerak, P.P. Pescarmona, Zeolites as selective adsorbents for CO_2 separation, ACS Appl. Energy Mater. 6 (2023) 2634–2656.

[3] Y. Li, J. Yu, Emerging applications of zeolites in catalysis, separation and host–guest assembly, Nat. Rev. Mater. 6 (2021) 1156–1174.

[4] Q. Lang, P. Lu, X. Yang, V. Valtchev, Zeolites for the environment, Green. Carbon 2 (2024) 12–32.

[5] R.M. Barrer, Hydrothermal Chemistry of Zeolites, Academic Press, London, 1982.

[6] A.-N. Parvulescu, S. Maurer, Toward sustainability in zeolite manufacturing: an industry perspective, Front. Chem. 10 (2022) 1050363.

[7] A. Chawla, A.J. Mallette, R. Jain, N. Le, F.C. Robles Hernández, J.D. Rimer, Crystallization of potassium-zeolites in organic-free media, Micropor. Mesopor Mater. 341 (2022) 112026.

[8] A.J. Mallette, G. Espindola, N. Varghese, J.D. Rimer, Highly efficient synthesis of zeolite chabazite using cooperative hydration-mismatched inorganic structure-directing agents, Chem. Sci. 15 (2024) 573–583.

[9] A.J. Mallette, K. Shilpa, J.D. Rimer, The current understanding of mechanistic pathways in zeolite crystallization, Chem. Rev. 124 (2024) 3416–3493.

[10] K. Asselman, N. Pellens, B. Thijs, N. Doppelhammer, M. Haouas, F. Taulelle, J. A. Martens, E. Breynaert, C.E.A. Kirschhock, Ion-pairs in aluminosilicate-alkali synthesis liquids determine the aluminum content and topology of crystallizing zeolites, Chem. Mater. 34 (2022) 7150–7158.

[11] K. Asselman, D. Vandenabeele, N. Pellens, N. Doppelhammer, C.E.A. Kirschhock, E. Breynaert, Structural aspects affecting phase selection in inorganic zeolite synthesis, Chem. Mater. 34 (2022) 11081–11092.

[12] E.B. Clatworthy, A.A. Paecklar, E. Dib, M. Debost, N. Barrier, P. Boullay, J.-P. Gilson, N. Nesterenko, S. Mintova, Engineering RHO nanozeolite: controlling the particle morphology, Al and cation content, stability, and flexibility, ACS Appl. Energy Mater. 5 (2022) 6032–6042.

[13] M. Debost, E.B. Clatworthy, J. Grand, N. Barrier, N. Nesterenko, J.-P. Gilson, P. Boullay, S. Mintova, Direct synthesis of nanosized CHA zeolite free of organic template by a combination of cations as structure directing agents, MicroMesoporousMater. 358 (2023) 112337.

[14] H. Yamada, H. Horikawa, C. Anand, K. Ohara, T. Ina, A. Machida, S. Tominaka, T. Okubo, Z. Liu, K. Iyoki, T. Wakihara, Atom-selective analyses reveal the structure-directing effect of Cs cation on the synthesis of zeolites, J. Phys. Chem. Lett. 14 (2023) 3574–3580.

[15] L. Tosheva, K. Garbev, G.J. Miller, B. Mihailova, Toward the synthesis of new zeolite structures in the presence of cesium: zeolite MMU-1, Cryst. Growth Des. 23 (2023) 3834–3844.

[16] X. Lu, M. Elimelech, abrication of desalination membranes by interfacial polymerization: history, current efforts, and future directions, Chem. Soc. Rev. 50 (2021) 6290–6307.

[17] D.M. Warsinger, S. Chakraborty, E.W. Tow, M.H. Plumlee, C. Bellona, S. Loutatidou, L. Karimi, A.M. Mikelonis, A. Achilli, A. Ghassemi, L.P. Padhye, S. A. Snyder, S. Curcio, C.D. Vecitis, H.A. Arafat, J.H. Lienhard V, A review of polymeric membranes and processes for potable waterreuse, Prog. Polym. Sci. 81 (2018) 209–237.

[18] W.J. Lau, A.F. Ismail, N. Misdan, M.A. Kassim, A recent progress in thin film composite membrane: a review, Desalination 287 (2012) 190–199.

[19] A.F. Ismail, M. Padaki, N. Hilal, T. Matsuura, W.J. Lau, Thin film composite membrane - Recent development and future potential, Desalination 356 (2015) 140–148.

[20] J.M. Gohil, P. Ray, A review on semi-aromatic polyamide TFC membranes prepared by interfacial polymerization: potential for water treatment and desalination, Sep. Purif. Technol. 181 (2017) 159–182.

[21] X. Wu, T. Chen, G. Dong, M. Tian, J. Wang, R. Zhang, G. Zhang, J. Zhu, Y. Zhang, A critical review on polyamide and polyesteramide nanofiltration membranes: emerging monomeric structures and interfacial polymerization strategies, Desalination 577 (2024) 117379.

[22] X. Zhang, H. Znahg, L. Wang, J. Wang, X. Wang, J. Hao, Probing the construction mechanism of polyamide membranes regulated by interfacial polymerization from the novel micro- and macro- perspectives: a review, Desalination 578 (2024) 117422.

[23] Z. Yang, H. Guo, Y. Tang, The upper bound of thin-film composite (TFC) polyamide membranes for desalination, J. Membr. Sci. 590 (2019) 117297.

[24] W.J. Lau, S. Gray, T. Matsuura, D. Emadzadeh, J.P. Chen, A.F. Ismail, A review on polyamide thin film nanocomposite (TFN) membranes: history, applications, challenges and approaches, Water Res. 80 (2015) 306–324.

[25] Z. Liao, J. Zhu, X. Li, B. Van der Bruggen, Regulating composition and structure of nanofillers in thin film nanocomposite (TFN) membranes for enhanced separation performance: a critical review, Sep. Purif. Technol. 266 (2021) 118567.

[26] X. Cui, G. Kong, S. Wei, Z. Zhang, Z. Kang, H. Guo, PolyMOF interlayers modulated interfacial polymerization of ultra-thin nanofiltration membranes with efficient and stable desalination performance, J. Membr. Sci. 702 (2024) 122780.

[27] S. Wei, Y. Guo, G. Yang, H. Guo, Z. Yan, S. Mintova, Q.J. Niu, EMT-NH_2 zeolite interlayer induces the formation of high-performance polyamide membrane, Chem. Eng. J. 472 (2023) 145081.

[28] D. Wang, M. Tian, S. Han, K. Ding, L. Yin, J. Zhu, Y. Zhang, L. Han, Enhanced performance of thin-film nanocomposite membranes achieved by hierarchical zeolites for nanofiltration, J. Membr. Sci. 671 (2023) 121405.

[29] J. Zhu, L. Qin, A. Uliana, J. Hou, J. Wang, Y. Zhang, X. Li, S. Yuan, J. Li, M. Tian, J. Lin, B. Van der Bruggen, Elevated performance of thin film nanocomposite membranes enabled by modified hydrophilic MOFs for nanofiltration, ACS Appl. Mater. Interfaces 9 (2017) 1975–1986.

[30] S. Wei, X. Ding, Y. Qiu, V. De Waele, H. Guo, Enhanced performance polyamide membrane by introducing high-porosity SOD/GO composite interlayer to tailor the interfacial polymerization process, Chem. Eng. J. 481 (2024) 148595.

[31] B.-H. Jeong, E.M.V. Hoek, Y. Yan, A. Subramani, X. Huang, G. Hurwitz, A. K. Ghosh, A. Jawor, Interfacial polymerization of thin film nanocomposites: a new concept for reverse osmosis membranes, J. Membr. Sci. 294 (2007) 1–7.

[32] M.L. Lind, A.K. Ghosh, A. Jawor, X. Huang, W. Hou, Y. Yang, E.M.V. Hoek, Influence of zeolite crystal size on zeolite-polyamide thin film nanocomposite membranes, Langmuir 25 (2009) 10139–10145.

[33] M. Fathizadeh, A. Aroujalian, A. Raisi, M. Fotouhi, Preparation and characterization of thin film nanocomposite membrane for pervaporative dehydration of aqueous alcohol solutions, Desalination 314 (2013) (2013) 20–27.

[34] S. Wei, H. Guo, X. Cui, X. Ding, X. Xia, V. de Waele, Fabrication of ultra-permeable membranes with antibiofouling capability by incorporating bifunctionalized zeolite, Sep. Purif. Technol. 354 (2025) 129258.

[35] F. Seyedpour, J. Farahbakhsh, Z. Dabaghian, W. Suwaileh, M. Zargar, A. Rahimpour, M. Sadrzadeh, M. Ulbricht, Y. Mansourpanah, Advances and challenges in tailoring antibacterial polyamide thin film composite membranes for water treatment and desalination: a critical review, Desalination 581 (2024) 117614.

[36] S. Malic, S. Rai, J. Redfern, J. Pritchett, C.M. Liauw, J. Verran, L. Tosheva, Zeolite-embedded silver extends antimicrobial activity of dental acrylics, Colloids Surf. B 173 (2019) 52–57.

[37] W. Wang, W. Li, Z. Wang, B. Liu, B. Wang, J. Duan, R. Zhou, Directly synthesized high-silica CHA zeolite for efficient CO_2/N_2 separation, J. Env. Chem. Eng. 12 (2024) 113036.

[38] S. Singh, K.C. Khulbe, T. Matsuura, P. Ramamurthy, Membrane characterization by solute transport and atomic force microscopy, J. Membr. Sci. 142 (1998) 111–127.

[39] S. Cao, L. Li, M. Guo, W. Xu, T. Liu, T. Xing, Z. Li, M. Wang, M. Wang, M. Wu, Construction of sunflower-like superstructure of CHA zeolite through oriented attachment for superior CO_2 separation performance via thermodynamic−kinetic synergistic adsorption, Chem. Mater. 35 (2023) 10119–10128.

[40] W. Gao, C.C. Amoo, G. Zhang, M. Javed, B. Mazonde, C. Lu, R. Yang, C. Xing, N. Tsubaki, Insight into solvent-free synthesis of MOR zeolite and its laboratory scale production, Micro Mesoporous Mater. 280 (2019) 187–194.

[41] V. Freger, Nanoscale heterogeneity of polyamide membranes formed by interfacial polymerization, Langmuir 19 (2003) 4791–4797.

[42] L. Tosheva, S. Belkhair, M. Gackowski, S. Malic, N. Al-Shanti, J. Verran, Rapid screening of the antimicrobial efficacy of Ag zeolites, Colloids Surf. B 157 (2017) 254–260.

[43] J. Redfern, K. Goldyn, J. Verran, R. Retoux, Lubomira Tosheva, S. Mintova, Application of Cu-FAU nanozeolites for decontamination of surfaces soiled with the ESKAPE pathogens, Micro Mesoporous Mater. 253 (2017) 233–238.

[44] F.N.S. Farah, T. Worthington, R.A. Martin, Biomed. Mater. 18 (2023) 045003.